



14-3-3 fusion oncogenes in high-grade endometrial stromal sarcoma

The MIT Faculty has made this article openly available. ***Please share*** how this access benefits you. Your story matters.

Citation	Lee, C.-H. et al. "14-3-3 Fusion Oncogenes in High-grade Endometrial Stromal Sarcoma." Proceedings of the National Academy of Sciences 109.3 (2012): 929–934. Copyright ©2012 by the National Academy of Sciences
As Published	http://dx.doi.org/10.1073/pnas.1115528109
Publisher	National Academy of Sciences
Version	Final published version
Accessed	Sat Jun 23 04:25:57 EDT 2018
Citable Link	http://hdl.handle.net/1721.1/72511
Terms of Use	Article is made available in accordance with the publisher's policy and may be subject to US copyright law. Please refer to the publisher's site for terms of use.
Detailed Terms	

14-3-3 fusion oncogenes in high-grade endometrial stromal sarcoma

Cheng-Han Lee^{a,b,1}, Wen-Bin Ou^{a,1}, Adrian Mariño-Enriquez^a, Meijun Zhu^a, Mark Mayeda^a, Yuexiang Wang^a, Xiangqian Guo^c, Alayne L. Brunner^c, Frédéric Amant^d, Christopher A. French^a, Robert B. West^c, Jessica N. McAlpine^e, C. Blake Gilks^b, Michael B. Yaffe^f, Leah M. Prentice^g, Andrew McPherson^g, Steven J. M. Jones^h, Marco A. Marra^h, Sohrab P. Shah^g, Matt van de Rijn^c, David G. Huntsman^g, Paola Dal Cin^a, Maria Debiec-Rychter^d, Marisa R. Nucci^a, and Jonathan A. Fletcher^{a,2}

^aDepartment of Pathology, Brigham and Women's Hospital, Boston, MA 02115; ^bDepartment of Pathology, Vancouver General Hospital, Vancouver, BC, Canada V5Z 4E3; ^cDepartment of Pathology, Stanford University Medical Center, Stanford, CA 94305; ^dCenter for Human Genetics, Catholic University of Leuven, B-3000 Leuven, Belgium; ^eDepartment of Gynecology and Obstetrics, University of British Columbia, Vancouver, BC, Canada V5Z 1M9; ^fDepartments of Biology and Biological Engineering, Koch Institute for Integrative Cancer Research, Massachusetts Institute of Technology, Cambridge, MA 02139; ^gCentre for Translational and Applied Genomics, British Columbia Cancer Agency, Vancouver, BC, Canada V5Z 4E6; and ^hMichael Smith Genome Sciences Centre, British Columbia Cancer Agency, Vancouver, BC, Canada V5Z 1L3

Edited by Bert Vogelstein, Johns Hopkins University, Baltimore, MD, and approved December 7, 2011 (received for review September 22, 2011)

14-3-3 proteins are ubiquitously expressed regulators of various cellular functions, including proliferation, metabolism, and differentiation, and altered 14-3-3 expression is associated with development and progression of cancer. We report a transforming 14-3-3 oncoprotein, which we identified through conventional cytogenetics and whole-transcriptome sequencing analysis as a highly recurrent genetic mechanism in a clinically aggressive form of uterine sarcoma: high-grade endometrial stromal sarcoma (ESS). The 14-3-3 oncoprotein results from a $t(10;17)$ genomic rearrangement, leading to fusion between 14-3-3 ϵ (YWHAE) and either of two nearly identical FAM22 family members (FAM22A or FAM22B). Expression of YWHAE-FAM22 fusion oncoproteins was demonstrated by immunoblot in $t(10;17)$ -bearing frozen tumor and cell line samples. YWHAE-FAM22 fusion gene knockdowns were performed with shRNAs and siRNAs targeting various FAM22A exons in an $t(10;17)$ -bearing ESS cell line (ESS1): Fusion protein expression was inhibited, with corresponding reduction in cell growth and migration. YWHAE-FAM22 maintains a structurally and functionally intact 14-3-3 ϵ (YWHAE) protein-binding domain, which is directed to the nucleus by a FAM22 nuclear localization sequence. In contrast to classic ESS, harboring JAZF1 genetic fusions, YWHAE-FAM22 ESS display high-grade histologic features, a distinct gene-expression profile, and a more aggressive clinical course. Fluorescence in situ hybridization analysis demonstrated absolute specificity of YWHAE-FAM22A/B genetic rearrangement for high-grade ESS, with no fusions detected in other uterine and nonuterine mesenchymal tumors (55 tumor types, $n = 827$). These discoveries reveal diagnostically and therapeutically relevant models for characterizing aberrant 14-3-3 oncogenic functions.

cytogenetic aberration | translocation | uterine neoplasm | NUT | leiomyosarcoma

The 14-3-3 protein family includes seven highly conserved dimeric isoforms (β , γ , ϵ , ζ , η , σ , and τ) that are expressed in all eukaryotic cells (1). Through interaction with phospho-serine or phospho-threonine motifs, 14-3-3 can regulate diverse cellular functions, including signal transduction, cytoskeletal configuration, metabolism, differentiation, survival, and transcription (2). 14-3-3 proteins are implicated in tumorigenesis (3, 4), as a tumor suppressor in the case of 14-3-3 σ (SFN), and as a putative oncoprotein in the case of 14-3-3 ζ (YWHAZ). 14-3-3 σ expression is inhibited in premalignant and malignant cells (5), and loss of 14-3-3 σ results in polyploidy and failure to maintain G2/M cell-cycle arrest after DNA damage through cytoplasmic sequestration of CDC2/cyclin B1 (6, 7). 14-3-3 ζ expression is up-regulated in various cancers (8), and it induces epithelial-mesenchymal transition by activation of TGF- β /Smads and inhibits apoptosis in anoikic cells, thereby potentiating tumor invasion and metastasis (9, 10). Although these observations demonstrate functional roles for altered expression of

14-3-3 in tumorigenesis, there have heretofore been no reported instances of genomically aberrant 14-3-3 oncogenes.

Endometrial stromal sarcoma (ESS) is a type of uterine sarcoma that, in its low-grade form, contains JAZF1 fusions with various polycomb complex proteins (SUZ12, PHF1, and EPC1) (11, 12). In contrast, some ESS are histologically high grade, and these tumors typically lack JAZF1 rearrangement. The genetic basis for high-grade ESS is undefined. In this study, we used a combination of conventional cytogenetics and next-generation sequencing to identify YWHAE-FAM22A/B genetic fusion as a frequent genetic event that is specific for high-grade ESS. We further demonstrated the transforming properties of the fusion protein and characterized the clinicopathologic significance of YWHAE-FAM22A/B genetic fusion. The discovery of this unique oncogenic mechanism has biologic, diagnostic, and therapeutic implications.

Results and Discussion

Conventional Cytogenetics and Whole-Transcriptome Sequencing Identifies YWHAE-FAM22A/B Fusion as a Frequent Recurrent Genetic Event in High-Grade ESS.

To characterize the genetic basis of high-grade ESS, we performed prospective cytogenetic G-banding analyses, which identified a translocation, $t(10;17)(q22;p13)$, as a recurrent and predominant aberration in 7 of 12 cases (Fig. 1A and Table S1). A spontaneously immortal cell line, ESS1, was established from one of these $t(10;17)$ -bearing ESS. Fluorescence in situ hybridization (FISH) localized the ESS 17p13 translocation breakpoint to the YWHAE (14-3-3 ϵ) gene (Fig. 1B). In contrast to the tumor cells, the adjacent normal myometrial tissues uniformly lacked YWHAE rearrangement by FISH, confirming the somatic nature of the rearrangement. One ESS had an unbalanced $t(10;17)$, associated with deletion of the rearranged YWHAE 3' end, thereby implicating the YWHAE 5' end in a putative $t(10;17)$ -associated fusion oncogene. FISH localizations mapped the 10q translocation breakpoint, in each $t(10;17)$ ESS, to one of two regions (10q22.3

Author contributions: C.-H.L., W.-B.O., C.A.F., M.B.Y., P.D.C., M.R.N., and J.A.F. designed research; C.-H.L., W.-B.O., A.M.-E., M.Z., M.M., Y.-X.W., X.G., A.L.B., J.N.M., L.M.P., P.D.C., M.D.-R., and M.R.N. performed research; C.-H.L., F.A., R.B.W., C.B.G., M.B.Y., M.A.M., S.P.S., M.v.d.R., D.G.H., P.D.C., M.D.-R., and J.A.F. contributed new reagents/analytic tools; C.-H.L., W.-B.O., A.M.-E., M.Z., X.G., A.L.B., R.B.W., J.N.M., C.B.G., A.M., S.J.M.J., M.A.M., S.P.S., M.v.d.R., D.G.H., and J.A.F. analyzed data; and C.-H.L., M.R.N., and J.A.F. wrote the paper.

The authors declare no conflict of interest.

This article is a PNAS Direct Submission.

Data deposition: The fusion gene sequences reported in this paper have been deposited in the GenBank database (accession nos. [JN999698](https://doi.org/10.1093/nar/gfr996) and [JN999699](https://doi.org/10.1093/nar/gfr999)).

¹C.-H.L. and W.-B.O. contributed equally to this work.

²To whom correspondence should be addressed. E-mail: jfletcher@partners.org.

This article contains supporting information online at www.pnas.org/lookup/suppl/doi:10.1073/pnas.1115528109/-DCSupplemental.

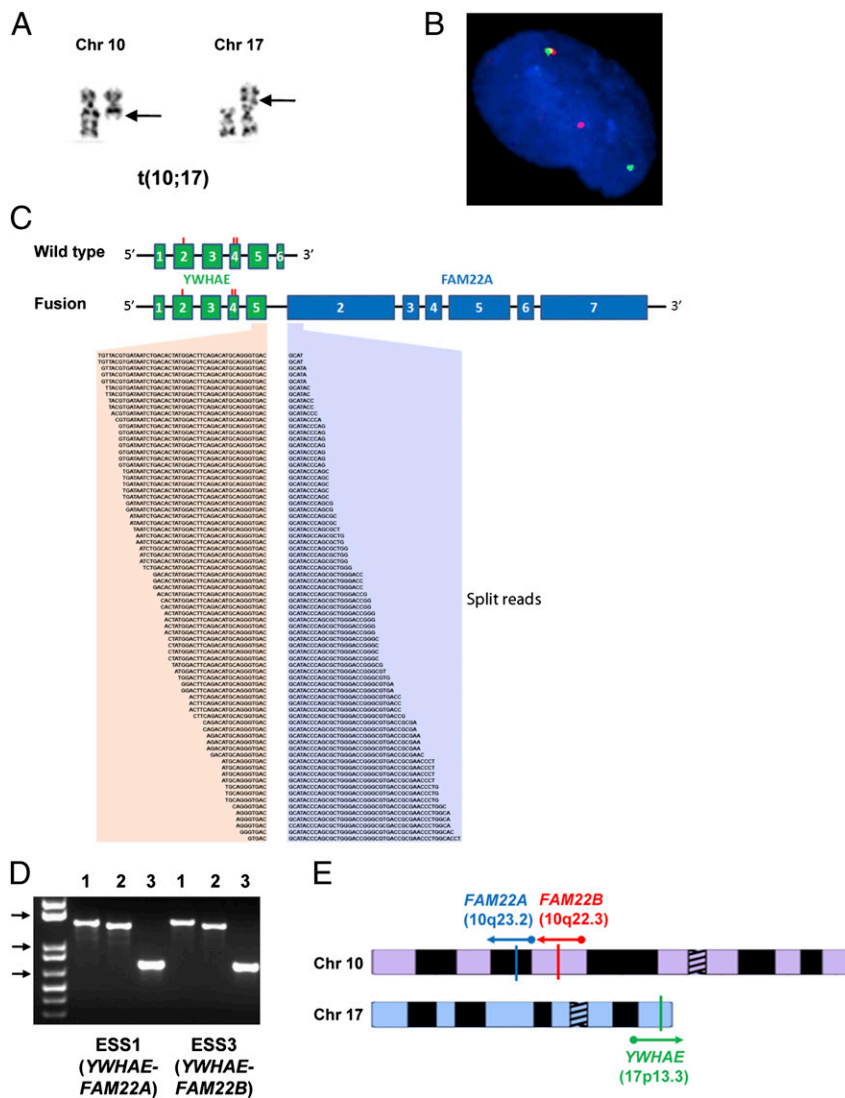


Fig. 1. Genomic mechanisms for the 14-3-3 fusion oncogene in endometrial cancer. (A) High-grade ESS G-banded partial karyotype showing a balanced translocation, $t(10;17)$. Arrows indicate the translocation breakpoints. (B) Split-apart view of *YWHAE*-flanking BACs, RP11-22G12 (red) and RP11-100F18 (green), demonstrates *YWHAE* rearrangement in an ESS1 cell. (C) deFuse analysis of ESS1 whole-transcriptome paired-end sequencing (Illumina) identifies split-read transcript sequences in which *YWHAE* exon 5 is fused to *FAM22A* exon 2. The conserved 14-3-3 protein-binding domains are encoded by exons 2 and 4 of *YWHAE* (denoted by the red lines). (D) RT-PCR using *YWHAE* exon 1 (lanes 1 and 2) and exon 5 (lane 3) forward primers with *FAM22A/B/E* exon 2 reverse primer in two $t(10;17)$ -bearing ESS. Sequence analyses showed *YWHAE-FAM22A* and *YWHAE-FAM22B*, respectively, in ESS1 and ESS3. The top, middle, and bottom arrows indicate 1,650-, 1,000-, and 650-Kb markers, respectively. (E) Schematic of *YWHAE* on chromosome 17 (Chr 17) and the two alternative fusion partners, *FAM22A* and *FAM22B* on chromosome 10 (Chr 10), with the direction of transcription indicated by arrows.

and 10q23.2) separated by 7.8 megabases (Fig. S1): notably, these regions had genomic and organizational similarities, each containing two members of the *FAM22* family. FISH mapping within these regions was hampered by the repetitive nature of the genomic sequences (Fig. S1). Because of the abundant expression of wild-type *YWHAE*, 3' RACE analysis was unsuccessful.

To demonstrate a putative *YWHAE* fusion oncogene in these genomically repetitive 10q regions, we used whole-transcriptome sequencing as an unbiased method. Sequencing was performed against the $t(10;17)$ -containing ESS1, and sequence reads were analyzed by using a custom-written deFuse algorithm designed to identify fusion transcripts in RNA sequencing datasets (13), including those involving members of highly homologous gene families. deFuse analysis identified in-frame *YWHAE-FAM22A* fusions of *YWHAE* exon 5 to *FAM22A* exon 2 (Fig. 1C and Table S2). *FAM22A* is located within the 10q23.2 breakpoint region, whereas the alternate breakpoint region, 10q22.3, contains *FAM22B* (encoding a protein with 99% amino acid identity to *FAM22A*) and *FAM22E*. RT-PCR with *YWHAE* forward primers and consensus reverse primers for *FAM22A/B/E* identified *YWHAE-FAM22B* fusion transcripts in each $t(10;17)$ ESS that lacked *YWHAE-FAM22A* (Fig. 1D). Therefore, *FAM22A* and *FAM22B* are alternative *YWHAE* gene fusion partners (Fig. 1E). In all cases, the genetic rearrangements in transcribed *YWHAE-FAM22* involved

fusion of *YWHAE* exon 5 to *FAM22A* or *FAM22B* exon 2, creating a fusion coding sequence consistent with genomic breakpoints in *YWHAE* intron 5 and *FAM22A/B* intron 1. *FAM22A* and *FAM22B* have sequence homology with *NUT*, an oncogene fused to *BRD4* and *BRD3* bromodomain genes in *NUT* midline carcinoma (14, 15). The *YWHAE-FAM22A* fusion transcript is 2,970 bp in length, and the corresponding protein product contains 989 aa, with a predicted molecular mass of 108 kDa (Dataset S1 and GenBank accession nos. JN999698 and JN999699).

***YWHAE-FAM22* Is Expressed in $t(10;17)$ -Bearing High-Grade ESS and Demonstrates Transforming Properties.** To identify expression of *YWHAE-FAM22A* and *YWHAE-FAM22B*, Western blotting was performed with N-terminal and C-terminal *YWHAE* antibodies, of which only the N-terminal antibody was expected to recognize the fusion proteins. Although both antibodies identified ~30-kDa wild-type *YWHAE* in all tumor samples examined, only the N-terminal *YWHAE* antibody identified putative *YWHAE-FAM22A/B* fusion proteins, which were represented in each $t(10;17)$ ESS by bands at 110 kDa and 140 kDa (Fig. S2). The 110-kDa form corresponds to the predicted molecular mass for *YWHAE-FAM22A/B*, whereas the 140-kDa form presumably represents a mature form of the fusion protein, after post-translational modifications. *YWHAE-FAM22A/B* expression was

considerably lower than that of the native YWHAE, in keeping with the whole-transcriptome sequence data that showed eight times fewer *YWHAE-FAM22A* reads than wild-type *YWHAE* reads in the breakpoint region. *YWHAE-FAM22A/B* oncoproteins were not detected in ESS or other sarcomas lacking *t(10;17)* nor were they detected in *t(10;17)* ESS by using antibodies to the YWHAE C-terminal region. Furthermore, endogenous ESS *YWHAE-FAM22A/B* fusion proteins comigrated with a FLAG-tagged *YWHAE-FAM22A* pcDNA3 construct expressed in HEK 293T cells (Fig. S2). These studies demonstrated equivalent *YWHAE-FAM22A/B* expression levels in *t(10;17)* ESS biopsy specimens compared with the ESS1 immortal cell line.

YWHAE-FAM22A oncogenic roles were evaluated in *t(10;17)* ESS1 cells by using shRNAs and siRNAs targeting *FAM22A*. *FAM22A* shRNA1 targets exon 2, which is contained in the fusion transcript. A control sequence, *FAM22A* shRNA2, targets exon 1, which is not in the fusion transcript, and is expected to inhibit wild-type *FAM22A/B/D/E*. The nonfusion transcript is minimal to absent in virtually all adult tissues and cancers (<http://www.ncbi.nlm.nih.gov/sites/entrez?db=unigene>), and ESS1 whole-transcriptome

sequencing showed that only 3% of reads in the breakpoint region were wild-type (unrearranged) *FAM22A*, whereas 97% were fusion *YWHAE-FAM22A*, indicating that wild-type *FAM22A* is expressed at low levels in ESS1. In contrast to empty vector and shRNA2, gene knockdown with shRNA1 inhibited *YWHAE-FAM22A* expression (110- and 140-kDa forms) in ESS1, with a corresponding reduction in viability and migration (Fig. S3). Similarly, ESS1 transfection with siRNAs targeting *FAM22A* exons 2 or 7 inhibited *YWHAE-FAM22A* expression, with corresponding reduction in ESS1 cell viability (Fig. S4). *YWHAE-FAM22A* transforming activity was further evaluated in mouse embryonic fibroblast 3T3 cells, where *YWHAE-FAM22A* but not *YWHAE* transfection induced cell viability and migration (Fig. 2A–C).

YWHAE-FAM22 Maintains 14-3-3 Binding Properties and Shows Aberrant Nuclear Localization. Structurally, the *YWHAE-FAM22A/B* oncoproteins contain an intact YWHAE protein-interaction domain (16), and loss of the YWHAE C-terminal end (encoded by *YWHAE* exon 6) and fusion to *FAM22A/B* are not predicted to functionally impair this rigid YWHAE protein-interaction domain or its ability to dimerize (Fig. 2D). Further analysis of *FAM22A/B* protein sequences revealed a bipartite nuclear localization sequence (Arg-805 to Arg-822) encoded by exons 7 of *FAM22A* and *FAM22B*. In contrast to native YWHAE protein, which is predominantly cytoplasmic (17), *YWHAE-FAM22A/B* was predicted to be predominantly nuclear (18–20). *YWHAE-FAM22A/B* nuclear localization was confirmed in ESS1 (Fig. 3A) and in 293T cells expressing a *YWHAE-FAM22A* construct (Fig. 3B).

YWHAE-FAM22 ESS Display Higher-Grade Histology and More Aggressive Clinical Course Compared with *JAZF1*-Rearranged ESS. Histologically, the 12 clinical cases of *YWHAE-FAM22A/B* ESS (Table S3) exhibited high-grade cytologic features compared with classic non-*t(10;17)* ESS (Fig. 4A). In contrast to *JAZF1*-rearranged ESS, which displayed uniform small round/oval nuclei and low proliferation rate (<5 mitotic figures per 10 high-power fields), *YWHAE-FAM22A/B* ESS showed enlarged nuclei with more irregular nuclear contour and high proliferation rate (>10 mitotic figures per 10 high-power fields). Gene-expression profiling by 3'

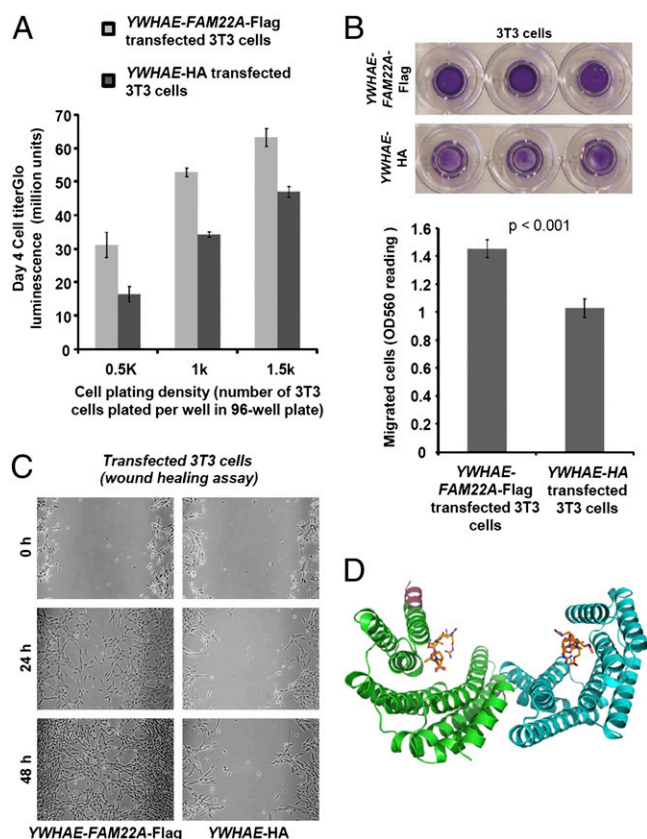


Fig. 2. Oncogenic roles of *YWHAE-FAM22A* fusion oncoprotein and structural considerations. (A) 3T3 cells transfected (Lipofectamine) with *YWHAE-FAM22A* pcDNA3 had increased cell viability (CellTiter Glo luminescence assay) at various plating densities compared with 3T3 cells transfected with *YWHAE* pcDNA3. Error bars indicate SEs. (B and C) 3T3 cells transfected (Lipofectamine) with *YWHAE-FAM22A* pcDNA3 migrated more rapidly than 3T3 cells transfected with *YWHAE* pcDNA3, as shown by assays for quantitative cell migration (B) and wound healing (C). Error bars indicate SEs. (D) Structural modeling of *YWHAE-FAM22A* (including the protein sequences encoded by exons 1 to ~5 of *YWHAE* and *FAM22A* exon 2) based on the X-ray crystal structure of 14-3-3. Heterodimer of *YWHAE-FAM22* bound to native YWHAE is depicted in stick representation. The green and cyan chains indicate YWHAE (14-3-3 ϵ) sequences with the purple helix representing the first part of *FAM22A*. This model shows that *YWHAE* fusion to *FAM22* is unlikely to interfere with YWHAE dimerization or phosphopeptide binding.

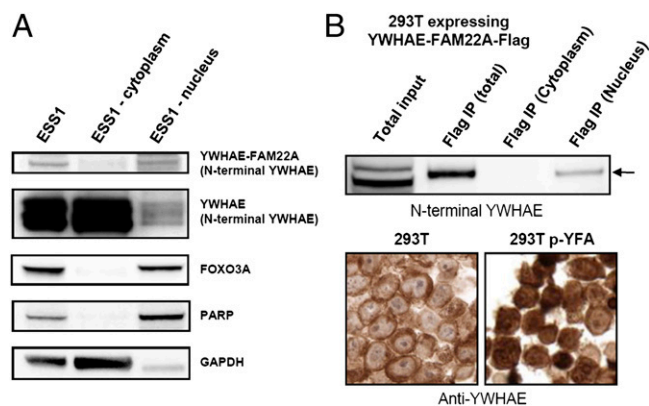


Fig. 3. Oncogenic fusion to *FAM22* enables aberrant nuclear localization of *YWHAE*. (A) Endogenous *YWHAE-FAM22A* is predominantly nuclear, whereas native *YWHAE* is predominantly cytoplasmic. FOXO3A and poly(ADP-ribose) polymerase (PARP) are nuclear localization controls, whereas GAPDH is a cytoplasmic control. (B) Induced *YWHAE-FAM22A* expression is nuclear in 293T cells, as shown by FLAG immunoprecipitation (Upper) and *YWHAE* immunohistochemistry (Lower) after transient expression of FLAG-tagged *YWHAE-FAM22A* pcDNA3 construct. In contrast to the predominantly cytoplasmic staining (and absent nuclear staining) seen in nontransfected 293T cells (representing wild-type *YWHAE*), *YWHAE* immunostaining in *YWHAE-FAM22A*-expressing 293T cells showed the presence of nuclear staining, indicating nuclear localization of the fusion protein.

mRNA sequencing demonstrated a distinctive expression profile in *YWHAE-FAM22A/B* ESS compared with *JAZF1*-rearranged ESS and uterine leiomyosarcoma (Fig. 4B). Genes involved in the regulation of cell proliferation (*CCND1* and *CEBPA*) and tissue invasion (*MMP15*, *FSCN1*, and *TIMP1*) were up-regulated in *YWHAE-FAM22A/B* ESS compared with *JAZF1*-rearranged ESS (Table S4). Clinically, patients with *YWHAE-FAM22A/B* ESS presented with higher-stage disease and experienced more frequent disease recurrence compared with patients with *JAZF1*-rearranged ESS (Fig. 4C and D). FISH analysis demonstrated absolute diagnostic specificity of *YWHAE-FAM22A/B* rearrangement for high-grade ESS (Table 1). In addition, *YWHAE-FAM22A/B* rearrangement and *JAZF1* rearrangement were mutually exclusive, and *YWHAE-FAM22A/B* rearrangement was not found in low-grade ESS ($n = 38$) or in various uterine and nonuterine mesenchymal tumors (55 tumor types, $n = 827$) (Table 1). These findings show that *YWHAE-FAM22A/B* rearrangement defines a group of uterine sarcomas that is genetically, histologically, and clinically distinct from classic *JAZF1*-rearranged ESS. This evidence prompts reconsideration of the current classification of endometrial sarcomas. In the present study, we refer to this genetically unique subgroup as *YWHAE-FAM22A/B* ESS. An alternative classification consideration would be “14-3-3 ESS,” which has the advantage of brevity while reflecting the expected biological contributions of *YWHAE* dysregulation. A biologic classification seems preferable to “high-

grade ESS,” which misleadingly suggest a biologic continuum with the genetically distinct *JAZF1* low-grade ESS.

In this study, we identified an oncogenic mechanism for 14-3-3 proteins in the form of a transforming *YWHAE-FAM22A/B* fusion oncoprotein. The translocation-mediated *YWHAE-FAM22A/B* fusions define a previously unrecognized group of uterine sarcoma, which is clinically more aggressive and histologically higher grade than *JAZF1*-rearranged ESS. *YWHAE-FAM22A/B* oncogenic fusion results in nuclear accumulation of the functionally intact *YWHAE* protein-interaction domain. Known cytoplasmic *YWHAE* protein-protein interactions are thereby likely redirected to the nuclear compartment. Disruption of *YWHAE* interaction in the nuclear compartment therefore would appear to be a rational therapeutic approach. This unique genetic fusion provides a compelling opportunity to characterize 14-3-3 functions in cancer development and progression.

Methods

Study Samples. The study samples include frozen and formalin-fixed paraffin-embedded tissues retrieved from tumor banks and pathology archives at Brigham and Women’s Hospital, Catholic University of Leuven, Vancouver General Hospital, and Stanford University Medical Center with the approval of the respective institutional research boards. Cell lines, including ESS1, ESS-JAZF1, gastrointestinal stromal tumor (GIST430), and leiomyosarcoma (LMS03), were developed at Brigham and Women’s Hospital.

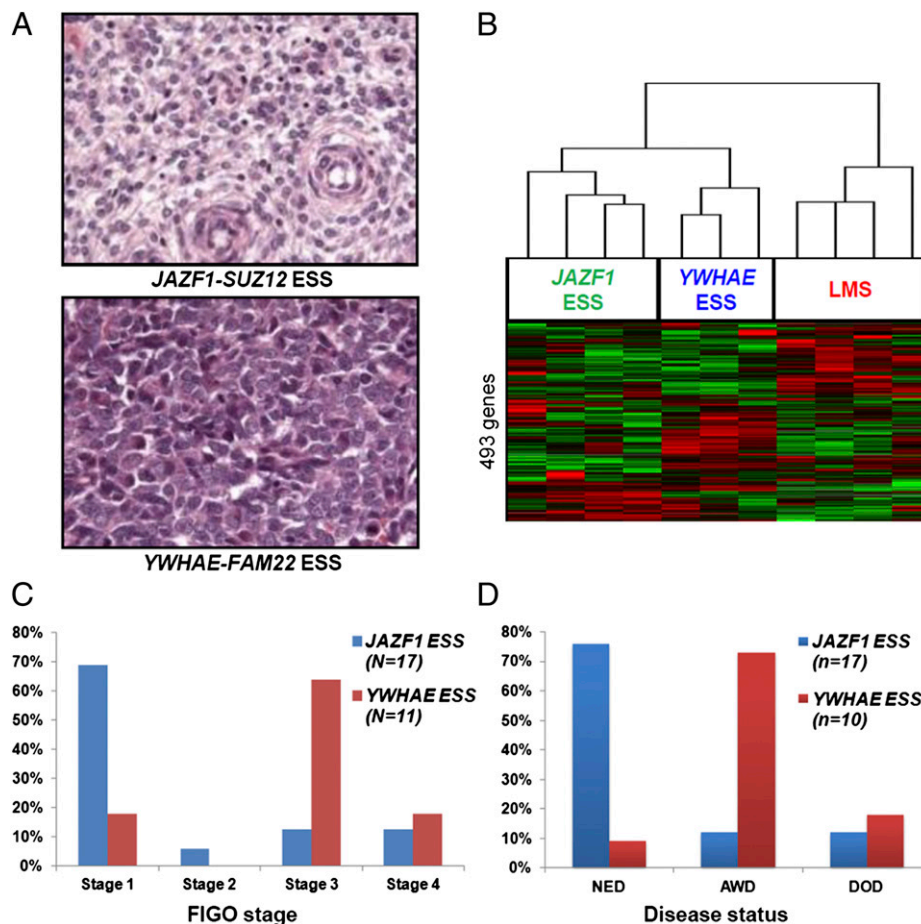


Fig. 4. *YWHAE-FAM22* ESS is associated with distinctive histology, gene-expression profiles, and clinical behavior. (A) *YWHAE-FAM22* ESS, in contrast to *JAZF1-SUZ12* ESS, has high-grade histology, with larger and more irregular nuclei and increased mitotic activity. (B) 3' sequencing gene-expression profiling with unsupervised hierarchical clustering demonstrates distinct gene-expression signatures between *YWHAE-FAM22* ESS (*YWHAE* ESS), *JAZF1*-rearranged ESS (*JAZF1* ESS), and uterine leiomyosarcoma (LMS). (C) Patients with *YWHAE-FAM22* ESS present with higher International Federation of Gynecology and Obstetrics (FIGO) stage disease compared with patients with *JAZF1*-rearranged ESS. (D) *YWHAE-FAM22* ESS (average follow-up period of 3.5 y) more frequently recurs compared with *JAZF1*-rearranged ESS (average follow-up period of 10 y). NED, no evidence of disease; AWD, alive with disease; DOD, died of disease.

Table 1. Specificity of *YWHAЕ-FAM22A/B* genetic rearrangement by FISH assays in uterine and extrauterine mesenchymal tumors (*n* = 827 cases, representing 55 tumor types)

FISH screen for <i>YWHAЕ-FAM22A</i> and <i>YWHAЕ-FAM22B</i>	No. of cases screened	No. of positive cases
Uterine lesions		
Classic ESS	38	0
Uterine adenocarcinoma/carcinosarcoma	16	0
Uterine leiomyosarcoma	105	0
Uterine leiomyoma	66	0
Polypoid endometriosis	7	0
Soft-tissue tumors		
Leiomyosarcoma	206	0
Undifferentiated pleomorphic sarcoma	59	0
Gastrointestinal stromal tumor	51	0
Desmoid type fibromatosis	22	0
Angiosarcoma	21	0
Solitary fibrous tumor	13	0
Dedifferentiated liposarcoma	12	0
Embryonal rhabdomyosarcoma	12	0
Synovial sarcoma	12	0
Dermatofibrosarcoma protuberans	10	0
Myxoid liposarcoma	10	0
Malignant peripheral nerve sheath tumor	7	0
Myxofibrosarcoma	6	0
Other benign and malignant mesenchymal tumors	154	0
Total	827	0

Cytogenetic Analysis and FISH. Cytogenetic analysis was performed on Giemsa-banded metaphase spreads per standard protocol (21). FISH analyses were performed on 4- μ m tissue sections that were prebaked for 2 h at 60 °C. The sections were deparaffinized in xylene three times for 15 min each and dehydrated twice in 100% ethanol for 2 min. The slides were immersed in Tris-EDTA [100 mM Tris base and 50 mM EDTA (pH 7.0)] for 45 min at 95–99 °C and rinsed in 1 \times PBS for 5 min. Proteolytic digestion of the sections was performed using Digest-ALL 3 (Invitrogen) at 37 °C for 20 min, twice. The sections were then sequentially dehydrated in alcohol (70%, 85%, 95%, and 100%) for 2 min each and air-dried. The *YWHAЕ* break-apart probe was composed of two sets of overlapping BAC clones (Children's Hospital Oakland Research Institute), telomeric (RP11-143L7 and RP11-22G12, biotin-labeled) and centromeric (RP11-100F18 and RP11-60C18, digoxigenin-labeled), detected with streptavidin Alexa Fluor 594 conjugate (Invitrogen) and FITC anti-digoxigenin (Roche Diagnostics). The 10q23.2 (*FAM22A* region) breakpoint flanking probes were RP11-1005L9 (biotin-labeled) and RP11-210E13 (digoxigenin-labeled), and the 10q22.3 (*FAM22B*-region) breakpoint flanking probes were RP11-715A21 (biotin-labeled) and RP11-668E21 (digoxigenin-labeled). One hundred nuclei per case were evaluated. Paired signals were defined as an orange and green signal less than two signal diameters apart or a single yellow (overlapping) signal, whereas unpaired signals were those separated by greater than or equal to two signal diameters. Only cases with clearly visible probe signals observed in at least 100 nuclei were considered interpretable. A case was considered to be positive for rearrangement if unpaired signals were seen in >20% of nuclei.

Paired-End RNA (Transcriptome) Sequencing and deFuse Analysis. RNA extraction and sequencing were performed as previously described (22–24). Double-stranded cDNA was synthesized from polyadenylated RNA, and the resulting cDNA was sheared. The 190- to 210-bp DNA fraction was isolated and PCR-amplified to generate the sequencing library, as per the Illumina Genome Analyzer paired-end library protocol (Illumina). The resulting libraries were sequenced on an Illumina GA II. Short read sequences obtained from the Illumina GA II were mapped to the reference human genome (NCBI build 36.1, hg18) plus a database of known exon junctions 2 by using MAQ 3 in paired-end mode.

Gene fusions were predicted with deFuse (13), which predicts gene fusions by searching paired-end RNA-sequencing data for reads that harbor fusion boundaries. Spanning reads harbor a fusion boundary in the unsequenced region in the middle of the read, whereas split reads harbor a fusion boundary in the sequence of one end. deFuse searched for spanning reads with read ends that align to different genes. Approximate fusion boundaries implied by spanning reads were then resolved to nucleotide level by using dynamic programming-based alignment of candidate split reads.

RT-PCR and Sequencing. RNAs from frozen tumor and cell line samples were extracted with a mirVana miRNA Isolation Kit (Ambion) according to the manufacturer's protocol. Reverse transcription was subsequently performed with an iScript cDNA Synthesis Kit to generate cDNA with 1 μ g of RNA sample. Forward primers specific for *YWHAЕ* (exon 1A: 5'-AGAGGCTGAGAGAGTC GGAGACA CTA-3'; exon 1B: 5'-TATGGATGATCGAGAGGATCTGGT-3'; and exon 5: 5'-CAGAAC TGGATACGC TGAGT GAAGAA-3') and a reverse primer specific for *FAM22A/B* (exon 2: 5'-CTCATAGACACT CCTGG GGTTACAGG-3') were used. PCR was performed with PCR SuperMix (11306; Invitrogen) according to the manufacturer's protocol with the following cycling conditions: 1 cycle at 94 °C for 2 min followed by 30 cycles of 94 °C for 0.5 min, 55 °C for 0.5 min, 68 °C for 2 min, and a final extension of 68 °C for 5 min. PCR products were evaluated on a 1% agarose gel alongside 1 Kb Plus DNA Ladder (Invitrogen) visualized with ethidium bromide staining. The PCR amplicon bands were excised from the gel, purified with a Qiagen Gel Purification Kit, and sequenced with BigDye Terminator v3.0 Ready Reaction Cycle Sequencing (Applied Biosystems) on an ABI PRISM 310.

Fusion Construct and Cloning. *YWHAЕ-FAM22A-FLAG* fusion cDNA containing BamHI (*YWHAЕ* end) and EcoRI (FLAG end) restriction sites was synthesized (GenScript) based on the sequences of the fusion transcript present in ESS1 and cloned in pUC57 vector. The fusion gene sequence was validated by sequencing. It was further subcloned in pCDNA3(+) by EcoRI and BamHI (GenScript). The construct integrity was verified by sequencing. The fusion construct was expressed in 293T cells by a Lipofectamine-based transfection method according to the manufacturer's instructions (Invitrogen Life Technologies).

Cell Lysate Preparation. Whole-cell lysates were prepared in lysis buffer [1% Nonidet P-40, 50 mM Tris-HCl (pH 8.0), 100 mM sodium fluoride, 30 mM sodium pyrophosphate, 2 mM sodium molybdate, 5 mM EDTA, and 2 mM sodium orthovanadate] containing protease inhibitors (10 μ g/mL aprotinin, 10 μ g/mL leupeptin, and 1 mM phenylmethylsulfonyl fluoride). Nuclear and cytoplasmic fraction lysates were prepared by using a Qproteome Cell Compartment Kit (Qiagen) according to the manufacturer's protocol. Protein concentrations were determined by using the Bio-Rad Protein Assay.

Western Blotting and Immunoprecipitation Studies. Electrophoresis and Western blotting were performed as described previously (25). In short, 30 μ g of protein was loaded on a 4–12% Bis-Tris gel (NuPAGE; Invitrogen) and blotted onto a nylon membrane. Immunoprecipitations were performed by incubating 1 mg of precleared cell lysate with anti-FLAG (mouse monoclonal, F1804; Sigma) for 2 h at 4 °C, followed by addition of 20 μ L of protein A Sepharose (Zymed Laboratories) for overnight incubation at 4 °C. The immunoprecipitates were

then washed three times with lysis buffer and one time with 750 μ L of 10 mM Tris (pH 7.4) buffer for 10 min each at 4 °C, before being resuspended in SDS/PAGE loading buffer containing 7.5% β -mercaptoethanol, heated at 95 °C for 5 min, resolved on 4–12% SDS/polyacrylamide gradient gels (NuPAGE; Invitrogen), and transferred to nylon membranes. Adequate protein transfer was demonstrated by staining the membranes with Ponceau S (Sigma Chemical).

The following primary antibodies were used for staining: antibodies raised against N-terminal (amino acids 1–70) YWHAE (rabbit polyclonal, HPA008445; Sigma) and against C-terminal (amino acids 239–255) YWHAE (rabbit polyclonal, BML-5A475R; Enzo Life Sciences), anti-FLAG (mouse monoclonal, F1804; Sigma), anti-FOXO3A (rabbit polyclonal, 9467; Cell Signaling), anti-poly(ADP-ribose) polymerase (PARP, mouse monoclonal, 33–3100; Zymed), and anti-GADPH (mouse monoclonal, G8795; Sigma). Detection was by ECL (Amersham Pharmacia Biotechnology) with a Fuji LAS1000 Plus chemiluminescence imaging system.

Preparation of Lentiviral FAM22A shRNA Constructs and Lentiviral Infections. FAM22A shRNAs were from Broad Institute RNAi Consortium: FAM22A shRNA1 (NM_001099338.1–3119s21c1), 5'-TCTTGCTGGGCCTTAGCTTTG-3'; and FAM22A shRNA2 (NM_001099338.1–598s21c1), 5'-TATGTTCCAGGAACCTGTTTA-3'. Lentiviral preparations were produced by cotransfecting empty vector pLKO.1 puro with FAM22A shRNA and helper virus packaging plasmids pCMV Δ R8.91 and vsv-g (at a 10:10:1 ratio) into 293T cells. Transfections were carried out with Lipofectamine and PLUS reagent. Lentiviruses were harvested at 24, 36, 48, and 60 h posttransfection. Viruses were frozen at –80 °C in aliquots at appropriate amounts for infection. ESS1 cells were seeded in 6-well plates. Infections were carried out in the presence of 8 μ g/mL polybrene. After transduction, ESS1 were selected with 2 μ g/mL puromycin for 15 d, then lysed for Western blot analysis. Cell culture images were obtained by using a Spot RT Slider Camera and Spot software (Version 4.6 for Windows) and a Nikon Eclipse TE2000-S inverted microscope.

In Vitro Wound-Healing Assays. Cell-wounding studies were carried out via standard methods (26). A slash was created in confluent cell cultures, using the tip of a P-100 Pipetman, at 8 d after shRNA transduction with puromycin selection. The plates were photographed at 0, 72, and 96 h with Spot software (Version 4.6 for Windows) and a Nikon Eclipse TE2000-S inverted microscope.

1. Aitken A (2006) 14-3-3 proteins: A historic overview. *Semin Cancer Biol* 16:162–172.
2. Mackintosh C (2004) Dynamic interactions between 14-3-3 proteins and phospho-proteins regulate diverse cellular processes. *Biochem J* 381:329–342.
3. Hermeking H (2003) The 14-3-3 cancer connection. *Nat Rev Cancer* 3:931–943.
4. Morrison DK (2009) The 14-3-3 proteins: Integrators of diverse signaling cues that impact cell fate and cancer development. *Trends Cell Biol* 19:16–23.
5. Lodygin D, Hermeking H (2006) Epigenetic silencing of 14-3-3 σ in cancer. *Semin Cancer Biol* 16:214–224.
6. Chan TA, Hermeking H, Lengauer C, Kinzler KW, Vogelstein B (1999) 14-3-3 σ is required to prevent mitotic catastrophe after DNA damage. *Nature* 401:616–620.
7. Wilker EW, et al. (2007) 14-3-3 σ controls mitotic translation to facilitate cytokinesis. *Nature* 446:329–332.
8. Neal CL, et al. (2009) 14-3-3 ζ overexpression defines high risk for breast cancer recurrence and promotes cancer cell survival. *Cancer Res* 69:3425–3432.
9. Li Z, et al. (2008) Down-regulation of 14-3-3 ζ suppresses anchorage-independent growth of lung cancer cells through anoikis activation. *Proc Natl Acad Sci USA* 105:162–167.
10. Lu J, et al. (2009) 14-3-3 ζ cooperates with ErbB2 to promote ductal carcinoma in situ progression to invasive breast cancer by inducing epithelial-mesenchymal transition. *Cancer Cell* 16:195–207.
11. Koontz JI, et al. (2001) Frequent fusion of the JAZF1 and JJAZ1 genes in endometrial stromal tumors. *Proc Natl Acad Sci USA* 98:6348–6353.
12. Micci F, Panagopoulos I, Bjerkehaugen B, Heim S (2006) Consistent rearrangement of chromosomal band 6p21 with generation of fusion genes JAZF1/PHF1 and EPC1/PHF1 in endometrial stromal sarcoma. *Cancer Res* 66:107–112.
13. McPherson A, et al. (2011) deFuse: An algorithm for gene fusion discovery in tumor RNA-Seq data. *PLoS Comput Biol* 7:e1001138.
14. French CA, et al. (2003) BRD4-NUT fusion oncogene: A novel mechanism in aggressive carcinoma. *Cancer Res* 63:304–307.
15. French CA, et al. (2008) BRD-NUT oncoproteins: A family of closely related nuclear proteins that block epithelial differentiation and maintain the growth of carcinoma cells. *Oncogene* 27:2237–2242.

3' End Sequencing Gene-Expression Analysis. We prepared 3' sequence libraries as previously described (27). Total RNA was purified from formalin-fixed paraffin-embedded sections after deparaffination with a xylene incubation, ethanol wash, and protease/DNase digestion (RecoverAll Total Nucleic Acid Isolation Kit; Ambion) per the manufacturer's protocol. Isolation of the mRNA 3' ends was achieved by oligo(dT) selection on 20 μ g of total RNA with the Oligotex mRNA Mini Kit (Qiagen). Insufficiently fragmented RNA was heat-sheared to ~100–200 bp. The poly(A)-selected RNA was then subjected to first- and second-strand cDNA synthesis and Illumina library synthesis. To obtain 36-base single-end sequence reads, 3'-end sequencing for expression quantification (3SEQ) libraries were sequenced with Illumina GA IIx machines. Reads were mapped first to the transcriptome (refMrna, downloaded from the UCSC genome browser, www.genome.ucsc.edu/) by using SOAP2, allowing at most two mismatches (28). Unmapped and nonuniquely mapping reads were then mapped against the human genome (hg19), also using SOAP2, and reads mapping to RefSeq exons (same strand) were determined. Total sequence reads for each gene symbol from the transcriptome mapping and genome mapping were summed to create the gene-expression profile matrix. The data were then normalized by expressing the number of reads as transcripts per million reads (TPM) and filtered to select genes with a value of ≥ 1 TPM in at least two samples and an absolute difference of ≥ 2 TPM across the series. From these genes, those with an SD ≥ 200 as determined by Cluster 3 software were log-transformed, centered by gene using Cluster 3 software, subjected to unsupervised hierarchical clustering by Centroid linkage, and visualized with Java TreeView. Significance analysis of microarrays (SAM; <http://www-stat.stanford.edu/~tibs/SAM/>) was used to identify genes expressed differentially between the tumor groups.

siRNA Study, Cell Viability Assay, and Quantitative Cell Migration Assay. The detailed methods are available in *SI Methods*.

ACKNOWLEDGMENTS. These studies were supported by the Virginia and Daniel K. Ludwig Trust for Cancer Research. Whole-transcriptome sequencing and analysis was supported by Terry Fox New Frontiers Program on the Genomics of Forme Fruste Tumours.

16. Gardino AK, Smerdon SJ, Yaffe MB (2006) Structural determinants of 14-3-3 binding specificities and regulation of subcellular localization of 14-3-3-ligand complexes: A comparison of the X-ray crystal structures of all human 14-3-3 isoforms. *Semin Cancer Biol* 16:173–182.
17. Brunet A, et al. (2002) 14-3-3 transits to the nucleus and participates in dynamic nucleocytoplasmic transport. *J Cell Biol* 156:817–828.
18. Brameier M, Krings A, MacCallum RM (2007) NucPred—predicting nuclear localization of proteins. *Bioinformatics* 23:1159–1160.
19. Briesemeister S, Rahnenführer J, Kohlbacher O (2010) Going from where to why—interpretable prediction of protein subcellular localization. *Bioinformatics* 26:1232–1238.
20. Nakai K, Horton P (1999) PSORT: A program for detecting sorting signals in proteins and predicting their subcellular localization. *Trends Biochem Sci* 24:34–36.
21. Fletcher JA, et al. (1991) Diagnostic relevance of clonal cytogenetic aberrations in malignant soft-tissue tumors. *N Engl J Med* 324:436–442.
22. Shah SP, et al. (2009) Mutation of FOXL2 in granulosa-cell tumors of the ovary. *N Engl J Med* 360:2719–2729.
23. Shah SP, et al. (2009) Mutational evolution in a lobular breast tumour profiled at single nucleotide resolution. *Nature* 461:809–813.
24. Wiegand KC, et al. (2010) ARID1A mutations in endometriosis-associated ovarian carcinomas. *N Engl J Med* 363:1532–1543.
25. Rubin BP, et al. (2001) KIT activation is a ubiquitous feature of gastrointestinal stromal tumors. *Cancer Res* 61:8118–8121.
26. Shaw RJ, et al. (2001) The Nf2 tumor suppressor, merlin, functions in Rac-dependent signaling. *Dev Cell* 1:63–72.
27. Beck AH, et al. (2010) 3'-end sequencing for expression quantification (3SEQ) from archival tumor samples. *PLoS ONE* 5:e8768.
28. Li R, et al. (2009) SOAP2: An improved ultrafast tool for short read alignment. *Bioinformatics* 25:1966–1967.